R. Vescovini, L. Dozio
A Variable-Kinematic Model for Variable Stiffness Plates: Vibration and Buckling Analysis
Composite Structures, Vol. 142, 2016, p. 15-26
doi:10.1016/j.compstruct.2016.01.068

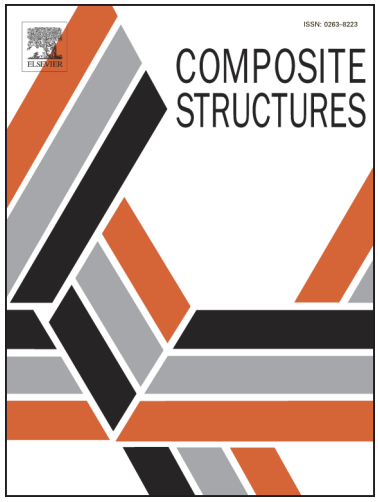

A Variable-Kinematic Model for Variable Stiffness Plates: Vibration and Buckling Analysis

Riccardo Vescovini, Lorenzo Dozio

PII: S0263-8223(16)00082-9
DOI: http://dx.doi.org/10.1016/j.compstruct.2016.01.068
Reference: COST 7174

To appear in: *Composite Structures*

Please cite this article as: Vescovini, R., Dozio, L., A Variable-Kinematic Model for Variable Stiffness Plates: Vibration and Buckling Analysis, *Composite Structures* (2016), doi: http://dx.doi.org/10.1016/j.compstruct.2016.01.068

A Variable-Kinematic Model for Variable Stiffness Plates: Vibration and Buckling Analysis

Riccardo Vescovini*and Lorenzo Dozio

Dipartimento di Scienze e Tecnologie Aerospaziali, Politecnico di Milano

Via La Masa 34, 20156 Milano, Italy

Abstract

This paper presents an advanced approximate technique for the vibration and buckling analysis of variable stiffness plates. The formulation is based on a variable-kinematic approach and is developed in the context of a variational framework together with the method of Ritz. Any set of boundary conditions can be accounted for, while loading conditions of pure axial compression are assumed. Results are validated against finite element predictions and solutions available in the literature, demonstrating the accuracy of the proposed method in terms of eigenvalues and modal shape descriptions. A novel set of vibration and buckling results is provided for moderately thick variable stiffness plates, including monolithic and sandwich configurations.

Keywords: variable stiffness; variable-kinematic theories; buckling; vibrations.

1 Introduction

In the past years, increasing interest has been devoted to the study of variable stiffness panels. As compared to classical straight fiber configurations, the adoption of a continuous variation of the stiffness properties can provide significant advantages. Indeed, the increased number of design variables extends the tailoring capabilities offered by composites, and requirements on stiffness, buckling and vibration behaviour can be strongly improved. One of the first investigations focusing on the potential benefits due to the stiffness variation is found in the work of Leissa and Martin [1]. The paper illustrates the possibility of improving

*Corresponding author. *Email address:* riccardo.vescovini@polimi.it (Riccardo Vescovini)

the buckling load and the fundamental frequency by as much as 38% and 21%, respectively. Solutions are derived using thin plate theory and the method of Ritz, and stiffness variation is achieved by means of non-uniformly spaced fibers. Another approach to obtain stiffness tailoring consists in varying the plate thickness. DiNardo and Lagace [2] investigated this strategy, and presented a Ritz-based methodology, in the context of thin-plate theory, to assess the bucking and post-buckling behaviour.

More often, stiffness tailoring has been achieved by considering curvilinear fiber configurations, which are also the subject of the present investigation. Back to the pioneering works of Hyer [3, 4] and Gürdal [5–7] and co-workers, many investigations have regarded the development of novel experimental, numerical and analytical methods to handle panels with curvilinear fibers. A comprehensive review can be found in Ref. [8]. Concerning the free vibrations, the number of investigations is relatively restricted and, in most cases, is based on a finite element approach. Abdalla et al. [9] proposed an optimization procedure to achieve the maximum fundamental frequency. The analysis is performed with finite elements based on Classical Lamination Theory (CLT), while lamination parameters are adopted to parametrize the design. The maximum frequency design of conical shells is the subject of Ref. [10], where finite element computations are performed with the commercial code Abaqus, and four node shell elements are used.

Honda and Narita [11] adopt eight-node, first-order finite elements in conjunction with genetic algorithms to maximize the fundamental frequency of locally anisotropic plates, including short and continuous curvilinear fibers. Natural frequencies and modes shapes are presented in the work of Akhavan and Ribeiro [12] using third-order shear deformation theory and taking manufacturing considerations into account. Results are presented for different combinations of boundary conditions, and are a useful benchmark for comparison purposes. In a recent paper, Tornabene et al. [13] presented high-order solutions for singly and doubly-curved panels with curvilinear fibers by means of the Local Generalized Differential Quadrature method.

The relatively large literature dealing with the buckling behavior of variable stiffness panels covers a number of numerical and semi-analytical investigations and, in most cases, CLT is adopted. An early work of Ref. [7] demonstrates the improvements in the buckling load thanks to the use of curvilinear fibers, and the implementation of the Ritz method is discussed in the context of CLT. Traditional finite element solutions, as well as highly efficient numerical techniques based on the Ritz technique, are established in Ref. [14].

The Galerkin method is implemented in Ref. [15] to solve the partial differential equations governing the buckling of thin variable stiffness plates. Setoodeh et al. [16] proposes the use of the reciprocal approximation for the buckling maximization of plates subjected to combined loading conditions. The method makes use of finite element computations based on CLT.

Semi-analytical solution strategies for the buckling analysis of variable angle tow panels, modeled using classical lamination plate theory are presented in Refs. [17, 18] and are based on the differential quadrature method (DQM) and the method of Ritz, respectively. The Ritz formulation is extended to the analysis of the post-buckling response in Ref. [19], where a mixed variational principle, expressed in terms of out of plane displacement and Airy stress function, is adopted [20, 21].

Among the few semi-analytical procedures for variable stiffness panels based on first-order theory, the works of Coburn at al. [22, 23] are here mentioned. They rely on the method of Ritz, where the stress function and the out of plane displacement are expanded using Legendre polynomials. The buckling of simply-supported blade stiffened panels is the subject of the research paper of Ref. [22], whereas sandwich plates with variable stiffness face-sheets are considered in Ref. [23]. This second study highlights the importance of the core shear modulus, illustrating that, below a threshold value, no tangible improvements can be achieved with respect to straight fiber configurations.

Despite the relatively large number of research studies dealing with the buckling and vibrations of variable stiffness plates, analytical and semi-analytical techniques have been mainly restricted to CLT and first-order theories. As a matter of fact, high-order solutions have been widely derived for straight fiber laminates using various approaches (see, for instance, [24–26]). In this context, a powerful approach to automatically handle a large variety of plate theories, including equivalent layer and layerwise theories of different order, is the so-called Carrera's Unified Formulation (CUF) [27, 28]. Within this framework, the exact solutions of the equations governing the buckling of simply-supported cross-ply plates is discussed in Refs. [29, 30], where the Navier and Lévy methods are applied.

Another interesting application of CUF regards its combined application with approximate techniques, an example of which is given by radial basis functions [31–33]. In these cases, strong form equations and boundary conditions are derived starting from the Principle of Virtual Discplacements (PVD), and the discretization is then performed on the basis of the interpolation technique of Ref. [34]. An application to the static and free vibration analysis of isotropic and cross-ply plates is found in Ref. [31], while buckling, bending and vibration response of functionally graded sandwich plates is discussed in Refs. [32, 33]. Recently, the combined use of radial basis functions and CUF has been extended to the buckling analysis of thin-walled beams [35].

Two other approximate techniques that have been successfully applied in the context of CUF are the Galerkin and the Modified Galerkin methods. They are applied in Refs. [36, 37] to obtain an extensive set of buckling and thermo-mechanical buckling solutions for multilayered simply-supported plates.

Still in the context of straight fiber plates, variable-kinematic formulations have been developed by solving

the weak form equations with the method of Ritz. Examples can be found for the buckling [36, 38] and vibration [39, 40] of composite plates.

To the best of the authors' knowledge, high-order solutions are still quite rare in the case of curvilinear fiber panels. The need for high-order solutions is additionally motivated by the fact that variable stiffness plates were found to be more affected by transverse shear effects than corresponding quasi-isotropic configurations [41]. Furthermore, large part of the works limits the analysis to simply-supported boundary conditions, while free and clamped conditions – and combinations of them – have been rarely assessed.

The present work aims to fill these gaps by presenting a novel semi-analytical approach for the analysis of variable stiffness panels. The theory relies on the use of CUF applied in conjunction with the method of Ritz. The resulting variable-kinematic approach is here denoted as vk-Ritz method.

Based on previous works by the authors for straight fiber panels [30, 38, 40, 42], the semi-analytical model has been extended to account for a continuous variation of the orientation angles in the space. The problem is developed by adopting a displacement-based approach, where the three components of the displacement field are expanded using Chebyshev polynomials and boundary characteristic functions. In the context of a variational framework, the set of equations governing the discrete problem is obtained for the buckling and free vibration analysis.

The vk-Ritz method is validated against results available in the literature, and is here adopted to present reference solutions, using theories of various order, for the buckling and vibrating modes of sandwich and monolithic variable stiffness panels.

2 Variable Stiffness Panels

The methodology is developed for the analysis of composite plates obtained by the stacking of plies with non-straight fibers; both thin and moderately thick plates are considered. A sketch of the panel is reported in Figure 1, where the reference system and the dimensions of the plate are illustrated. In particular, the panel is characterized by length a and width b. It is obtained by the stacking of a number N_l of plies, each one characterized by thickness h_k, for a total thickness equal to h.

A Cartesian coordinate system is taken such that the x-axis is directed parallel to the longitudinal edge of length a, and the y-axis is parallel to the transverse edge of length b. The four sides of the panel are numbered in a counterclockwise direction, as reported in Figure 1.

The four panel edges can be subjected to any combination of clamped, simply-supported and free boundary

conditions, while the loading case, for the buckling analysis, is restricted to the pure axial compression.

Different approaches can be assumed to express the fiber angle variation: Lobatto and Lagrange polynomials [18, 43], NURBS [44], or linear interpolation within control points [10] are few but examples. In this study, the fiber angle is allowed to vary along the x or the y direction with a linear law, but it is never function of both the coordinates. Therefore, stiffness variation can be achieved along one of the two directions. In case of fiber variation along the x axis, the orientation angle at a generic point of the panel domain is expressed as [6]:

$$\theta(x) = \frac{2\,(T_1 - T_0)}{a}|x| + T_0 \tag{1}$$

where T_0 is the orientation angle at the center of the panel, i.e. $x = 0$, while T_1 is the fiber orientation at the panel edge, i.e. $x = \pm a/2$. By integration of Eq. (1), the coordinates y of the fiber passing through the origin are obtained as:

$$y = \frac{a}{2\,(T_0 - T_1)} \left\{ \ln \left| \cos \left[\frac{2\,(T_1 - T_0)}{a} x + T_0 \right] \right| - \ln \left| \cos\left(T_0\right) \right| \right\} \qquad \text{if } x > 0 \tag{2}$$

$$y = \frac{a}{2\,(T_1 - T_0)} \left\{ \ln \left| \cos \left[\frac{2\,(T_0 - T_1)}{a} x + T_0 \right] \right| - \ln \left| \cos\left(T_0\right) \right| \right\} \qquad \text{if } x < 0 \tag{3}$$

Similar equations are easily derived for the case of fiber orientations varying along the direction y. To illustrate the path of a generic fiber passing through the center of the plate, a sketch is presented in Figure 2. The fiber orientation angles are positive in the counterclockwise direction, according to the notation of Figure 2. As outlined by Akhavan and Ribeiro [12], two strategies can be implemented to place the other fibers starting from the reference path, namely the parallel and the shifted method. The former consists in placing the fibers such that each point lies at constant distance from the reference fiber, the latter consists in translating the reference fiber along, in this case, the y axis. In this study, it is assumed that the shifted method is adopted for the fiber placement.

Following the classical notation for variable stiffness panels [45], the layer $<T_0|T_1>$ denotes a fiber path with orientation angle varying from T_0, at the center of the panel, to T_1 at the panel edge, as illustrated in Figure 2. To clearly distinguish between fiber variation along the x and y direction, a subscript is added, so that $[<T_0|T_1>_x]$ is a ply with fiber variation along x, and $[<T_0|T_1>_y]$ is a ply with fiber variation along y.

Regarding the vibration analysis, no assumptions are introduced on the stacking sequence of the laminate. In this case, any kind of elastic coupling is accounted for, including those due to membrane or flexural anisotropy, as well as those arising from unsymmetric stacking sequences.

For the buckling analysis, the class of laminates is restricted to the case of symmetric and balanced laminates.

In any case, this assumption is not too restrictive as typical aeronautical panels are commonly designed under the constraint of symmetric stacking and null in-plane anisotropy.

3 Variable-Kinematic Formulation

The variable-kinematic model is developed by adopting a variational approach. The problem is stated starting from the Lagrangian of the system, which reads:

$$L = T - U \tag{4}$$

where U is the strain energy an T is the kinetic energy. In particular, the strain energy associated to the plate of Figure 1 is written as:

$$U = \frac{1}{2}\sum_{k=1}^{N_l}\int_\Omega\int_{z_k}^{z_{k+1}} \left({\boldsymbol{\epsilon}_p^k}^T \boldsymbol{\sigma}_p^k + {\boldsymbol{\epsilon}_n^k}^T \boldsymbol{\sigma}_n^k + {\boldsymbol{\epsilon}_{p_{nl}}^k}^T \boldsymbol{\sigma}_{p0}^k \right) \mathrm{d}z \ \mathrm{d}\Omega \tag{5}$$

where Ω denotes the domain $[-a/2 \quad a/2] \times [-b/2 \quad b/2]$. The first two contributions are due to the internal work of in-plane and normal stress components, while the third contribution accounts for the initial state of stress, hereinafter denoted as pre-buckling state.

In the expression of Eq. (5), the components of the deformation and stress tensors are split into the in-plane and normal contributions, according to the definitions:

$$\boldsymbol{\epsilon}_p^k = \left\{ \epsilon_{xx}^k \quad \epsilon_{yy}^k \quad \gamma_{xy}^k \right\}^{\mathrm{T}} \qquad \boldsymbol{\sigma}_p^k = \left\{ \sigma_{xx}^k \quad \sigma_{yy}^k \quad \tau_{xy}^k \right\}^{\mathrm{T}} \tag{6}$$

$$\boldsymbol{\epsilon}_n^k = \left\{ \gamma_{xz}^k \quad \gamma_{yz}^k \quad \epsilon_{zz}^k \right\}^{\mathrm{T}} \qquad \boldsymbol{\sigma}_n^k = \left\{ \tau_{xz}^k \quad \tau_{yz}^k \quad \sigma_{zz}^k \right\}^{\mathrm{T}} \tag{7}$$

and the vector accounting for the initial stress state is defined as:

$$\boldsymbol{\sigma}_{p0}^k = \left\{ \sigma_{0xx}^k \quad \sigma_{0yy}^k \quad \tau_{0xy}^k \right\}^{\mathrm{T}} \tag{8}$$

The three components of Eq. (8) define the pre-buckling state of the plate and are determined from an initial linear analysis, whose details are discussed later. The work-conjugated term to Eq. (8) is the nonlinear part of the Green-Lagrange strain tensor, which is expressed as:

$$\boldsymbol{\epsilon}_{p_{nl}}^k = \left\{ \begin{array}{c} \frac{1}{2}\left[\left(u_{,x}^{k\,2} + v_{,x}^{k\,2} \right) \varphi + w_{,x}^{k\,2} \right] \\ \frac{1}{2}\left[\left(u_{,y}^{k\,2} + v_{,y}^{k\,2} \right) \varphi + w_{,y}^{k\,2} \right] \\ \left(u_{,x}^k u_{,y}^k + v_{,x}^k v_{,y}^k \right) \varphi + w_{,x}^k w_{,y}^k \end{array} \right\} \tag{9}$$

where the scalar φ is null if von Kármán approximation is adopted, and is equal to one otherwise; the terms u^k, v^k and w^k are the components of the displacement field. In the notation here adopted, the comma followed by an index denotes differentiation with respect to that index. The expression of the kinetic energy reads:

$$T = \frac{1}{2}\sum_{k=1}^{N_l}\int_\Omega\int_{z_k}^{z_{k+1}} \rho^k \dot{\mathbf{u}}^{k\mathrm{T}}\dot{\mathbf{u}}^k \,\mathrm{d}z\,\mathrm{d}\Omega \tag{10}$$

where the dot denotes the time derivative, ρ^k is the k-th ply density, and the displacement vector $\mathbf{u}^k$ is:

$$\mathbf{u}^k = \begin{Bmatrix} u^k & v^k & w^k \end{Bmatrix}^{\mathrm{T}} \tag{11}$$

The formulation is developed in the context of a displacement-based approach, so the ply constitutive equation and the strain-displacement relations are introduced to express the strain energy U as function of the displacement components.

Referring to the vector-like organization of the stress and strain components of Eqs. (6) and (7), the ply constitutive law, expressed in the global reference system, reads:

$$\begin{aligned} \boldsymbol{\sigma}_p^k &= \tilde{\mathbf{C}}_{pp}^k(x,y)\,\boldsymbol{\epsilon}_p^k + \tilde{\mathbf{C}}_{pn}^k(x,y)\,\boldsymbol{\epsilon}_n^k \\ \boldsymbol{\sigma}_n^k &= \tilde{\mathbf{C}}_{np}^k(x,y)\,\boldsymbol{\epsilon}_p^k + \tilde{\mathbf{C}}_{nn}^k(x,y)\,\boldsymbol{\epsilon}_n^k \end{aligned} \tag{12}$$

where the matrices $\tilde{\mathbf{C}}_{ik}$ are functions of the position due to the steering of fibers.

In a similar fashion, the strain-displacement relations are expressed as:

$$\begin{aligned} \boldsymbol{\epsilon}_p^k &= \mathbf{D}_p\mathbf{u}^k \\ \boldsymbol{\epsilon}_n^k &= \mathbf{D}_n\mathbf{u}^k + \frac{\partial}{\partial z}\mathbf{u}^k \end{aligned} \tag{13}$$

where the differential operators $\mathbf{D}_p$ and $\mathbf{D}_n$ are defined as:

$$\mathbf{D}_p = \begin{bmatrix} (\cdot)_{,x} & 0 & 0 \\ 0 & (\cdot)_{,y} & 0 \\ (\cdot)_{,y} & (\cdot)_{,x} & 0 \end{bmatrix} \qquad \mathbf{D}_n = \begin{bmatrix} 0 & 0 & (\cdot)_{,x} \\ 0 & 0 & (\cdot)_{,y} \\ 0 & 0 & 0 \end{bmatrix} \tag{14}$$

The total potential energy is re-written by substituting Eqs. (12)-(14) into Eq. (5). The expression so obtained is:

$$\begin{aligned} U = \frac{1}{2}\sum_{k=1}^{N_l}\int_\Omega\int_{z_k}^{z_{k+1}} \Bigg\{ &\left(\mathbf{D}_p\mathbf{u}^k\right)^{\mathrm{T}}\left[\tilde{\mathbf{C}}_{pp}^k\mathbf{D}_p\mathbf{u}^k + \tilde{\mathbf{C}}_{pn}^k\left(\mathbf{D}_n\mathbf{u}^k + \mathbf{u}_{,z}^k\right)\right] + \\ + &\left(\mathbf{D}_n\mathbf{u}^k + \mathbf{u}_{,z}^k\right)^{\mathrm{T}}\left[\tilde{\mathbf{C}}_{np}^k\mathbf{D}_p\mathbf{u}^k + \tilde{\mathbf{C}}_{nn}^k\left(\mathbf{D}_n\mathbf{u}^k + \mathbf{u}_{,z}^k\right)\right] + \boldsymbol{\epsilon}_{p_{nl}}^{k^T}\boldsymbol{\sigma}_{p0}^k \Bigg\}\,\mathrm{d}z\,\mathrm{d}\Omega \end{aligned} \tag{15}$$

The last term of Eq. (15), which is due to the pre-buckling state, can be conveniently re-written as:

$$\boldsymbol{\epsilon}_{p_{nl}}^{k^T}\boldsymbol{\sigma}_{p0}^{k} = \left(\mathbf{D}_{nl}\mathbf{u}^{k}\right)^{\mathrm{T}}\boldsymbol{\Sigma}_{p0}^{k}\mathbf{D}_{nl}\mathbf{u}^{k} \tag{16}$$

with:

$$\mathbf{D}_{nl} = \begin{bmatrix} (\cdot)_{,x} & 0 & 0 \\ (\cdot)_{,y} & 0 & 0 \\ 0 & (\cdot)_{,x} & 0 \\ 0 & (\cdot)_{,y} & 0 \\ 0 & 0 & (\cdot)_{,x} \\ 0 & 0 & (\cdot)_{,y} \end{bmatrix} \tag{17}$$

$$\boldsymbol{\Sigma}_{p0}^{k} = \begin{bmatrix} \varphi\boldsymbol{\sigma}_{p0}^{k} & 0 & 0 \\ 0 & \varphi\boldsymbol{\sigma}_{p0}^{k} & 0 \\ 0 & 0 & \boldsymbol{\sigma}_{p0}^{k} \end{bmatrix} \qquad \boldsymbol{\sigma}_{p0}^{k} = \begin{bmatrix} \sigma_{0xx} & \tau_{0xy} \\ \tau_{0xy} & \sigma_{0yy} \end{bmatrix} \tag{18}$$

It is worth observing that, in the present study, the pre-buckling stress is described by considering only the in-plane components σ_{0xx}, σ_{0yy} and τ_{0xy}. For many practical situations, including the case of a symmetric and balanced laminate loaded in compression, the other stress components are effectively null. However, no restriction exists in extending the presented approach to consider a more complex pre-buckling state.

After substitution of Eq. (16) into Eq. (15), the displacement-based expression of the total potential energy is obtained as:

$$\begin{aligned} U = \frac{1}{2}\sum_{k=1}^{N_l}\int_{\Omega}\int_{z_k}^{z_{k+1}} \Bigg\{ & \left(\mathbf{D}_p\mathbf{u}^k\right)^{\mathrm{T}}\left[\tilde{\mathbf{C}}_{pp}^{k}\mathbf{D}_p\mathbf{u}^k + \tilde{\mathbf{C}}_{pn}^{k}\left(\mathbf{D}_n\mathbf{u}^k + \mathbf{u}_{,z}^k\right)\right] + \\ & + \left(\mathbf{D}_n\mathbf{u}^k + \mathbf{u}_{,z}^k\right)^{\mathrm{T}}\left[\tilde{\mathbf{C}}_{np}^{k}\mathbf{D}_p\mathbf{u}^k + \tilde{\mathbf{C}}_{nn}^{k}\left(\mathbf{D}_n\mathbf{u}^k + \mathbf{u}_{,z}^k\right)\right] + \\ & + \left(\mathbf{D}_{nl}\mathbf{u}^k\right)^{\mathrm{T}}\boldsymbol{\Sigma}_{p0}^{k}\mathbf{D}_{nl}\mathbf{u}^k \Bigg\}\,\mathrm{d}z\,\mathrm{d}\Omega \end{aligned} \tag{19}$$

3.1 Displacement field approximation

By adopting Carrera's unified formulation and using its well-known notation (see, for instance, Ref. [27, 28]), the displacement field is approximated, by separation of variables, as:

$$\mathbf{u}^k(\xi,\eta,\zeta) = F_\tau(\zeta)\,\mathbf{u}_\tau^k(\xi,\eta) \tag{20}$$

where the nondimensional coordinates ξ and η are introduced by the transformation of coordinates:

$$\xi = \frac{2x}{a} \qquad \eta = \frac{2y}{b} \tag{21}$$

The repeated index τ of Eq. (20) implies the summatory according to the Einsten's convention. The term F_τ denotes the thickness function and depends on the kind of theory adopted, as well as its order. In particular, a set of equivalent layer theories, denoted as EDn, is obtained by assuming F_τ as a set of polynomial functions defined by:

$$F_\tau = \zeta^\tau \quad \text{with} \quad \tau = 0, 1, \ldots, N \tag{22}$$

where ζ is the nondimensional thicknesswise coordinate defined in [-1 1].

A set of layerwise theories, denoted as LDn, can be derived by assuming, for each ply composing the lay-up, the following set of functions:

$$F_t = \frac{1+\zeta_k}{2}; \quad F_b = \frac{1-\zeta_k}{2}; \quad F_r = P_r\left(\zeta_k\right) - P_{r-2}\left(\zeta_k\right) \quad \text{with} \quad r = 2, \ldots, N \tag{23}$$

where P_r are Legendre polynomials of order r.

According to the approach proposed by Dozio and Carrera [40], the generalized displacement components $\mathbf{u}_\tau^k$ are approximated with a Ritz-like expansion as:

$$\mathbf{u}_\tau^k\left(\xi,\eta\right) = \begin{bmatrix} N_{u\tau i} & 0 & 0 \\ 0 & N_{v\tau i} & 0 \\ 0 & 0 & N_{w\tau i} \end{bmatrix} \begin{Bmatrix} c_{u\tau i}^k \\ c_{v\tau i}^k \\ c_{w\tau i}^k \end{Bmatrix} = \mathbf{N}_{\tau i}\mathbf{c}_{\tau i}^k \tag{24}$$

The admissible functions $N_{l\tau i}$ are those relative to the component l of the displacement, and are chosen according to the boundary conditions. Assuming the separation of the variables, they are represented as:

$$N_{l\tau i}\left(\xi,\eta\right) = \Phi_{l\tau m}\left(\xi\right)\Psi_{l\tau n}\left(\eta\right) \quad \text{with} \quad m, n = 1, \ldots, P \tag{25}$$

and, in turn, the functions Φ and Ψ are obtained as:

$$\Psi_{u\tau n}\left(\eta\right) = g_{u\tau}\left(\xi\right)p_n\left(\eta\right) \quad \Phi_{u\tau m}\left(\xi\right) = f_{u\tau}\left(\xi\right)p_m\left(\eta\right) \tag{26}$$

where f and g are boundary compliant functions whose definition can be found in Ref. [40], and the terms p_l are Chebyshev polynomials given by:

$$p_l = \cos\left[\left(l-1\right)\arccos\left(\xi\right)\right] \tag{27}$$

The expression of the strain energy, under the approximation of the Ritz method, is obtained after substituting Eqs. (20)-(27) into Eq. (19) as:

$$U = \frac{1}{2}\sum_{k=1}^{N_l}\sum_{\tau,s=1}^{N}\sum_{i,j=1}^{M}\mathbf{c}_{\tau i}^{k^{\mathrm{T}}}\left(\mathbf{K}_{\tau sij}^k + \mathbf{G}_{\tau sij}^k\right)\mathbf{c}_{sj}^k \tag{28}$$

where $\mathbf{K}^k_{\tau sij}$ and $\mathbf{G}^k_{\tau sij}$ are the so-called Ritz fundamental nuclei [40] of the stiffness and geometric stiffness matrices, respectively, whose expression is obtained as:

$$\begin{aligned}\mathbf{K}^k_{\tau sij} = \int_{-1}^{1}\int_{-1}^{1} \left(\mathbf{D}_p\mathbf{N}_{\tau i}\right)^{\mathrm{T}} \left(E^k_{\tau s}\tilde{\mathbf{C}}^k_{pp}\mathbf{D}_p\mathbf{N}_{sj} + E^k_{\tau s}\tilde{\mathbf{C}}^k_{pn}\mathbf{D}_n\mathbf{N}_{sj} + E^k_{\delta\tau s}\tilde{\mathbf{C}}^k_{pn}\mathbf{N}_{sj}\right) + \\ + \left(\mathbf{D}_n\mathbf{N}_{\tau i}\right)^{\mathrm{T}} \left(E^k_{\tau s}\tilde{\mathbf{C}}^k_{np}\mathbf{D}_p\mathbf{N}_{sj} + E^k_{\tau s}\tilde{\mathbf{C}}^k_{nn}\mathbf{D}_n\mathbf{N}_{sj} + E^k_{\delta\tau s}\tilde{\mathbf{C}}^k_{nn}\mathbf{N}_{sj}\right) + \\ + \mathbf{N}^{\mathrm{T}}_{\tau i} \left(E^k_{\delta\tau s}\tilde{\mathbf{C}}^k_{np}\mathbf{D}_p\mathbf{N}_{sj} + E^k_{\delta\tau s}\tilde{\mathbf{C}}^k_{nn}\mathbf{D}_n\mathbf{N}_{sj} + E^k_{\delta\tau\delta s}\tilde{\mathbf{C}}^k_{nn}\mathbf{N}_{sj}\right) \frac{ab}{4}\,\mathrm{d}\xi\,\mathrm{d}\eta\end{aligned} \tag{29}$$

$$\mathbf{G}^k_{\tau sij} = \int_{-1}^{1}\int_{-1}^{1} \left(\mathbf{D}_{nl}\mathbf{N}_{\tau i}\right)^{\mathrm{T}} \mathbf{\Sigma}^k_{p0}\mathbf{D}_{nl}\mathbf{N}_{sj}E^k_{\tau s}\frac{ab}{4}\,\mathrm{d}\xi\,\mathrm{d}\eta \tag{30}$$

Similarly, the maximum kinetic energy associated to an harmonic motion of the plate is:

$$T = \frac{\omega^2}{2}\sum_{k=1}^{N_l}\sum_{\tau,s=1}^{N}\sum_{i,j=1}^{M} \mathbf{c}^{k^{\mathrm{T}}}_{\tau i}\mathbf{M}^k_{\tau sij}\mathbf{c}^k_{sj} \tag{31}$$

where the mass matrix nucleus reads:

$$\mathbf{M}^k_{\tau sij} = \int_{-1}^{1}\int_{-1}^{1} E_{\tau s}\rho^k\mathbf{N}^{\mathrm{T}}_{ti}\mathbf{N}_{sj}\frac{ab}{4}\,\mathrm{d}\xi\,\mathrm{d}\eta \tag{32}$$

and ω is the circular frequency. The full expressions of the 3×3 nuclei of Eqs. (29), (30) and (32) are provided in the Appendix.

The governing equations are obtained by expanding the nuclei over the indexes τ, s, i and j, and are assembled according to the procedure outlined in Ref. [40]. By imposing the first variation of the functional of Eq. (4) to vanish, the governing equations are obtained as:

$$\left(-\omega^2\mathbf{M} + \mathbf{K} + \mathbf{G}\right)\mathbf{c} = \mathbf{0} \tag{33}$$

which is the eigenvalue problem corresponding to the vibration analysis of a plate in presence of a pre-load. The natural vibration problem of the unloaded plate is derived from Eq. (33) by considering null loading stiffness $\mathbf{G}$, and so:

$$\left(-\omega^2\mathbf{M} + \mathbf{K}\right)\mathbf{c} = \mathbf{0} \tag{34}$$

The buckling problem can be recovered from Eq. (33) by introducing the unknown multiplier of the pre-buckling condition λ. The eigenvalue problem is then:

$$\left(\mathbf{K} + \lambda\mathbf{G}\right)\mathbf{c} = \mathbf{0} \tag{35}$$

From the solution of Eqs. (34) and (35), the modal and the buckling shapes are obtained as the eigenvectors of the problem, while the eigenvalues correspond to the square of the angular frequency and the buckling

multiplier, respectively. It is worth noting that the buckling problem is, in general, non-positive definite, and the buckling condition is that one corresponding to the smallest positive eigenvalue.

3.2 Pre-buckling Analysis

Under specific assumptions regarding the boundary conditions and the fiber steering law, the pre-buckling condition can be obtained in a closed-form manner with no need to solve the linear static problem numerically. A discussion regarding the linear response of variable stiffness panels is found in Ref. [6, 45].

In this paper, it is assumed that the panel is loaded with an imposed edge displacement equal to Δu, uniform along the transverse edges, while the longitudinal edges are free to translate, but forced to remain straight. The assumption of straight edges is representative of the typical deformation pattern of the skin of stringer-stiffened panels, where the in-plane bending stiffness of the stringers forces the skin edges to remain straight [46, 47]. A picture illustrating the loading condition and the pre-buckling deformation pattern is given in Figure 3.

Depending on whether the orientation angle varies along the x- or y-axis (Case A and Case B, respectively), two distinct, exact, pre-buckling solutions can be determined as outlined in the following.

Case A - Orientation angle variable along x

This pre-buckling configuration corresponds to a panel with stiffness variation along the axis x, therefore not allowing for load redistribution along the width when a displacement is imposed along the x-direction. Referring to the approach proposed by Gürdal and Olmedo [6], the in-plane force resultants are obtained as:

$$\begin{aligned} N_x &= N_0 \\ N_y &= \frac{A_{12}(x)}{A_{11}(x)} N_0 - \frac{A_{22}(x)A_{11}(x) - A_{12}(x)^2}{A_{11}(x)} \frac{c}{d} N_0 \\ N_{xy} &= 0 \end{aligned} \tag{36}$$

where N_0 denotes the constant in-plane compressive force per unit length associated to the imposed displacement Δu. The in-plane stiffness terms A_{ik} are defined as:

$$A_{11} = \sum_{k=1}^{N_l} \left(\tilde{C}_{11}^k - \frac{\tilde{C}_{13}^{k^2}}{\tilde{C}_{33}^k} \right) h_k \quad A_{12} = \sum_{k=1}^{N_l} \left(\tilde{C}_{12}^k - \frac{\tilde{C}_{13}^k \tilde{C}_{23}^k}{\tilde{C}_{33}^k} \right) h_k \quad A_{22} = \sum_{k=1}^{N_l} \left(\tilde{C}_{22}^k - \frac{\tilde{C}_{23}^k \tilde{C}_{23}^k}{\tilde{C}_{33}^k} \right) h_k \tag{37}$$

and the scalar terms c and d are given by the expressions:

$$\begin{aligned} c &= \int_0^{a/2} \frac{A_{12}(x)}{A_{11}(x)}\,\mathrm{d}x \\ d &= \int_0^{a/2} \frac{A_{22}(x)A_{11}(x) - A_{12}(x)^2}{A_{11}(x)}\,\mathrm{d}x \end{aligned} \tag{38}$$

The results of Eq. (36) illustrate that the axial force resultant is constant over the entire panel domain, and the shear load is identically null. The stiffness variation along x and the in-plane boundary condition of straight longitudinal edges determine the onset of a non null transverse force per unit length N_y, and whose resultant is zero.

The relation between the imposed axial displacement and the force resultant N_0 can be derived as:

$$\Delta u = \int_{-a/2}^{a/2} \frac{d + cA_{12}(x)}{A_{11}(x)d}\,\mathrm{d}x\, N_0 \tag{39}$$

Case B - Orientation angle variable along y

Case B deals with variable stiffness panels characterized by a steering of the fibers along the y-direction. From the compressive buckling point of view, this is the most interesting configuration. Indeed, the possibility of tailoring the fiber angle in the transverse direction can be exploited to achieve load redistribution at the panel edges, with consequent improvements on the buckling load.

In this case, the closed-form solution for the pre-buckling stress resultants is:

$$\begin{aligned} N_x &= \left[A_{11}(y) - \frac{A_{12}(y)^2}{A_{22}(y)}\right]\frac{\Delta u}{a} \\ N_y &= 0 \\ N_{xy} &= 0 \end{aligned} \tag{40}$$

As opposed to Case A, not only the shear resultant N_{xy} is null, but also the transverse in-plane forces are null, meaning that no reacting forces are needed to enforce the condition of straight edges.

In this case, the panel stiffness is not constant in the transverse direction and, accordingly, the profile of the axial force N_x varies along the y-coordinate, as seen from the first of Eq. (40). It is then useful to introduce the average value of the axial force per unit length carried by the panel as:

$$N_{x,\mathrm{avg}} = \frac{1}{b}\int_{-b/2}^{b/2} N_x(y)\,\mathrm{d}y \tag{41}$$

3.3 Ply stresses

Once the in-plane stress resultant are available from Eq. (36) or Eq. (40), the ply stresses are determined referring to the ply constitutive law and assuming vanishing stress σ_{0zz}:

$$\begin{aligned}
\sigma^k_{0xx} &= \left(\tilde{C}^k_{11} - \frac{\tilde{C}^{k\,2}_{13}}{\tilde{C}^k_{33}}\right)\epsilon_{0xx} + \left(\tilde{C}^k_{12} - \frac{\tilde{C}^k_{23}\tilde{C}^k_{13}}{\tilde{C}^k_{33}}\right)\epsilon_{0yy} \\
\sigma^k_{0yy} &= \left(\tilde{C}^k_{12} - \frac{\tilde{C}^k_{13}\tilde{C}^k_{23}}{\tilde{C}^k_{33}}\right)\epsilon_{0xx} + \left(\tilde{C}^k_{22} - \frac{\tilde{C}^{k\,2}_{23}}{\tilde{C}^k_{33}}\right)\epsilon_{0yy} \\
\sigma^k_{0xy} &= \left(\tilde{C}^k_{16} - \frac{\tilde{C}^k_{13}\tilde{C}^k_{36}}{\tilde{C}^k_{33}}\right)\epsilon_{0xx} + \left(\tilde{C}^k_{26} - \frac{\tilde{C}^{k\,2}_{23}\tilde{C}^k_{36}}{\tilde{C}^k_{33}}\right)\epsilon_{0yy}
\end{aligned} \tag{42}$$

where the shear deformations γ_{0xy} are identically null due to the assumption of balanced laminate. The longitudinal and transverse deformations, which are equal for each ply of the laminate, are:

$$\begin{aligned}
\epsilon_{0xx} &= \frac{1}{A_{11}A_{22} - A^2_{12}}\left(A_{22}N_x - A_{12}N_y\right) \\
\epsilon_{0yy} &= \frac{1}{A_{11}A_{22} - A^2_{12}}\left(-A_{12}N_x + A_{11}N_y\right)
\end{aligned} \tag{43}$$

The ply stresses, as determined from Eq. (42), are substituted into Eq. (30) and the expression of the geometric stiffness nucleus is determined.

4 Results

The results obtained with the vk-Ritz method are presented with regard to the vibration and buckling analysis of a number of variable stiffness panels. To check the accuracy of the predictions, the results are compared with those available in the literature and with Abaqus finite element analyses. To this aim, high-fidelity S4R shell elements are used.

A set of novel results is proposed for various combinations of boundary conditions and using theories of different orders, including equivalent layer and layerwise approaches. The panels under investigation are not restricted to the case of monolithic constructions, but include also sandwich panels with variable stiffness face-sheets. Due to the lack of refined solutions for variable stiffness plates, these results are an interesting reference for future studies in this field.

For monolithic plates and sandwich face-sheets, two aerospace CFRP materials are assumed. More specifically, Material 1 is assumed in the context of vibration analyses, while Material 2 is considered for buckling analyses. The elastic properties of these two materials are summarized in Table 1.

For Material 1, the orthotropy ratio E_{11}/E_{22} is equal to 24 and, for Material 2, it is 14. As discussed in the next, thick variable stiffness panels can undergo local, undesired, buckling modes much more frequently than straight fiber configurations. For this reason, materials with higher values of orthotropy ratio, which in fact would tend to promote local buckling modes, are not accounted for.

Regarding the cores of the sandwich constructions, two distinct materials are considered, so that the effect of varying the core stiffness can be assessed. Both the configurations are 5052 alloy hexagonal aluminum honeycombs [48], with a typical cell size of 1/8 in., and differing each other by the foil thickness.

The first configuration is a high density core, henceforth denoted as Core H, with a foil thickness equal to 0.003 in. The second configuration, denoted as Core L, has a thickness of 0.001 in. and, consequently, lower density.

The mechanical properties of the two cores are determined following the approach proposed by Burton and Noor [49], where the aluminum foil properties are taken as E=72 GPa and ν=0.3. Note that the transverse shear stiffness G_{13} here considered is the upper bound prediction obtained with the approach proposed in Ref. [49]. The elastic properties of the two cores are summarized in Table 2. It can be observed that the transverse shear properties of the configuration Core H are, approximately, three times higher if compared to the properties of the Core L.

4.1 Vibration analysis

A preliminary study is carried out to find the number of shape functions guaranteeing the convergence of the results. To this aim, a simply-supported square plate with width-to-thickness ratio of 50 is considered. The plate is made of Material 1 and ED4 plate theory is adopted. With the aim of highlighting the effect of varying the stiffness on the convergence properties of the solution, two lay-ups are considered. The first plate is a straight fiber cross-ply configuration with stacking sequence $[0\ 90]_s$. The second plate is a variable stiffness laminate with lay-up $[\pm<0|90>_x]_s$. This second configuration is intentionally characterized by high degree of fiber curvature in order to exacerbate the effects due to the fiber steering. The results are summarized in Table 3, where the first four nondimensional frequencies are reported by varying the number of shape functions from P=4 up to 14. Note that an equal number of functions along the two orthogonal directions x and y is assumed in all the cases. The percent values in the parenthesis denote the difference with respect to the frequency obtained in the previous run, using a smaller number of functions.

It is observed that, as expected, the results converge monotonically in both cases. Moreover, the first configuration displays faster convergence properties and, by taking P=10, the maximum difference with

respect to the previous frequency value is 0.02%. For the variable stiffness plate, a value of P=10 is associated to a maximum percent difference of 0.85% with respect to the results obtained considering P=8. When the number of functions is increased to P=12, the maximum difference reduces to 0.28% and, for$P$=14, the difference is 0.20%.

A good compromise between accuracy of the predictions and size of the problem is obtained by choosing a number of functions such that the maximum difference is below 0.50%. According to this threshold value, the number of function is taken equal to P=12.

Comparison with literature and finite elements

Free vibrations are investigated by presenting the comparison with the results of Refs. [12, 13]. The panel is made of Material 1 and has dimensions a and b equal to 1000 mm × 1000 mm. The laminate is obtained by the stacking of three plies at [<0|45>$_x$, <-45|-60>$_x$, <0|45>$_x$]. The stacking sequence is symmetric but unbalanced, therefore the laminate exhibits bending/twisting elastic coupling. The total thickness h is taken equal to 10 mm and 100 mm, so that the effect of different width-to-thickness ratios can be assessed.

The comparison between theories of various order is summarized in Table 4 for a panel subjected to simply-supported conditions at the four edges. The table reports also the frequencies obtained by Ribeiro et al. [8] using a third-order finite element formulation – here taken as reference to compute the percent differences reported in the parenthesis – and those of Tornabene and co-workers [13], obtained with a fourth-order theory and LGDQ method.

For the thin plate configuration, i.e. b/h=100, the differences between the results obtained with EDn and LDn theories are almost null. As expected, no improvement in the quality of the results is achieved by increasing the order of the theory, as the response of a thin plates is accurately captured by low-order EDn theories. Good agreement is observed with the results of Refs. [12, 13].

Different considerations can be drawn for the panel with b/h=10, where the adoption of the ED2 theory leads to errors higher than 4.0%. On the other hand, ED3 and ED4 guarantee close matching with the results of Ref. [12, 13], with slightly smaller frequency values. It is interesting to highlight that LD1 results are characterized by a maximum percent difference close to 2%, and the corresponding frequencies are higher if compared with ED3 and ED4 theory. As a matter of fact, the enforcement of a linear behaviour along the thickness has a detrimental effect on the results, despite the approach is layerwise.

On the other hand, LD2 and LD3 theories lead to frequency values that are slightly smaller in comparison to those obtained with ED4 theory and to the frequencies presented in Ref. [12] using a third-order shear

deformation theory.

Additional results are summarized in Table 5 considering, in this case, clamped boundary conditions along the four edges. Again, close matching is observed for all the theories when b/h=100. For the thicker configuration with b/h=10, it can be seen that ED2 theory is responsible for relatively large errors. At least, ED3 theory is needed to guarantee a good level of accuracy of the results. Even in this case, the frequencies obtained with LD1 theory are higher in comparison to ED3 and ED4.

Further results are provided for the natural frequencies and vibrating modes of sandwich plates with variable stiffness face-sheets. In particular, the lay-up and the material of the face-sheets are the same of the previous examples, while the low density honeycomb of Table 2 is taken as core material. The ratio between the face-sheet thickness h_{f} and the total thickness h is fixed to 0.10. The first four nondimensional frequencies are presented in Table 6 for different width-to-thickness ratio b/h and a/b, while the first four vibrating modes are plotted in Figure 4 for a square plate with b/h=100 and various boundary conditions.

Despite the presence of the core, plates with b/h=100 can be accurately described using ED2 theory. Contrarily, ED4 theory is needed to avoid large errors when b/h is reduced to 50. In these conditions, the adoption of a layerwise theory does not offer any substantial advantages in comparison to ED4 theory. The opposite can be said for thicker plates with b/h=10, where the maximum differences between ED4 and LD2 can be as high as 3%.

4.2 Buckling analysis

The second part of the work deals with the buckling analysis of variable stiffness sandwich panels. In this context, the face-sheets are made of Material 2, while the effect of the core stiffness is assessed by considering the two materials of Table 2.

As in the case of vibration analysis, the convergence of the method is checked by progressively increasing the number of shape functions, and evaluating the percent differences with the results obtained in the previous run. To highlight how convergence is affected by the non-uniformity of the panel stiffness, two configurations are considered. The first panel is cross-ply, straight-fiber laminate, with stacking sequence $[0\ 90]_{\mathrm{s}}$; the second plate has variable stiffness and lay-up $[\pm\!<\!90|0\!>_y]_{\mathrm{s}}$. It is worth highlighting that this second configuration does not account for any manufacturing constraint regarding the fiber curvature, but is artificially considered to achieve drastic stiffness variation.

Simply-supported boundary conditions are assumed, and the ratio b/h is fixed to 50. The results of the convergence analysis, obtained by considering ED4 theory, are presented in Table 7. It is interesting to

highlight the faster convergence in the case of the straight fiber configuration. In particular, the buckling load of the cross-ply laminate reaches convergence for P equal to 8, while this is not the case for the second configuration.

Considering the same threshold value of 0.50% used before for the free vibration analysis, the number of functions is fixed to P=12. It is reminded that realistic variable stiffness configurations are generally characterized by milder stiffness variation in comparison to the lay-up of Table 7 . Therefore, their convergence properties can be reasonably expected to be something in between the two cases of Table 7.

A set of results is derived for sandwich configurations characterized by various geometric ratios, lay-ups and boundary conditions. Due to the lack of available benchmark results for variable stiffness sandwich panels, all the buckling loads are compared with Abaqus finite element predictions.

A preliminary analysis was conducted to ensure that the plate undergoes global instability. Indeed, the failure modes of thick variable stiffness panels – as opposed to straight fiber configurations – tend to be dominated by core crushing mechanisms and highly localized modes. This behaviour, which is exacerbated by fiber steering configurations leading to noticeable load redistribution towards the edges, is not desirable from a design point of view. Furthermore, the present vk-Ritz approach can hardly predict local modes efficiently, as the shape functions are defined at global level. Therefore, a careful selection of the ply orientations is needed to ensure that the buckling modes are of global type.

For the first sandwich configuration, the stacking sequence is taken equal to $[\pm<45|30>_y]_s$. In addition to guaranteeing a global instability mechanism, this is an attractive configuration as it is characterized by improved buckling loads with respect to the straight fiber ± 45 configuration. The steering of the fiber from 45 to 30 degrees determines a beneficial pre-buckling load redistribution and leads to higher bifurcation loads. Nondimensional buckling loads are reported in Table 8 for thin and moderately thick square plates, and four different boundary conditions are considered. Furthermore, the ratio between the face-sheet and the total plate thickness is varied from 0.05 to 0.10.

In general, good agreement between LD1, LD2 and Abaqus buckling loads can be observed for all the results of Table 8. Regarding EDn theories, the accuracy of the results is restricted to a subset of cases, as discussed here below. In particular, ED2 theory leads to an over-prediction of the buckling load that can be as high as 5%, even in the case of thin sandwich plates with b/h=100. Fourth order ED4 theory seems adequate for the analysis of plates with b/h=100, but is responsible for a maximum error of 3% when the width-to-thickness ratio is increased to 50. Contrarily, accurate predictions are obtained by adopting a layerwise LD1 and LD2 approach, although no substantial improvements are obtained when the order of the layerwise description

is increased from 1 to 2. All the cases reported in Table 8 clearly illustrate that fully clamped boundary conditions are those responsible for the highest differences between plate theories. On the opposite, simply-supported plates are less sensitive.

In addition, it is observed that the difference between ED2 and higher order results increases with the ratio h_{F}/h.

The results of Tables 9 and 10 provide an assessment of the effect of different core stiffness and face-sheet lay-up. The nondimensional parameters b/h and h_{F}/h are fixed to 50 and 0.10, respectively.

The results of Table 9 are presented for the straight fiber lay-up $[\pm 45]_2$, and for two variable stiffness configurations with fiber variation along the direction y. The first lay-up is $[<45|30>_y]_{\mathrm{s}}$ and is characterized by a mild fiber steering; the second, $[<75|15>_y]_{\mathrm{s}}$, displays an aggressive steering which has the effect of promoting a drastic pre-buckling stress redistribution towards the edges and, consequently, higher buckling loads. A plot of the buckling modes is provided in Figure 5 with regard to the configuration with lay-up $[<45|30>_y]_{\mathrm{s}}$ and Core H. Similar shapes, although not reported here, are obtained for all the configurations of Table 9.

Additional results are proposed in Table 10 by considering face-sheets with fiber steering along the x-direction, thus corresponding to Case A pre-buckling condition. In this case, load redistribution towards the edges cannot be achieved, but a beneficial transverse tensile internal force allows improved buckling response with respect to the straight fiber configuration. As seen from the results of Tables 9 and 10, fully clamped and simply-supported plates are the most and less sensitive boundary conditions to the plate theory adopted, respectively.

It is interesting to note that, despite the ratio b/h is not particularly small, ED2 leads to unacceptable errors in all the cases here presented. Referring to the fully clamped panel, the errors range from 2% to 22%.

Both in Tables 9 and 10, ED4 theory provides accurate predictions only for Core H material. In this case, the maximum difference with respect to FEM results remains below 1%. However, the error increases up to 4% when the core stiffness is reduced, and Core L is assumed. Therefore, it is concluded that the use of EDn theories, despite the clear advantages from a computational point of view, is not an appropriate choice when dealing with sandwich variable stiffness panels. For relatively stiff cores, ED4 could be used but, to a more general extent, a layerwise theory is the most appropriate strategy.

Finally, it is remarked that the accuracy of the results seems independent on the amount of fiber curvature, and similar percent differences are obtained for corresponding configurations with different lay-up.

5 Conclusions

The paper has proposed a variable-kinematic approach based on the combined use of CUF and the Ritz method for the vibration and buckling analysis of variable stiffness plates.

The present vk-Ritz formulation offers the major advantage of making it possible the analysis of any combination of boundary conditions. Furthermore, high-order and layerwise theories are embedded in the formulation thanks to the unified approach. Therefore, refined vibration and buckling results can be obtained for panels characterized by small width-to-thickness ratios and, in the case of sandwich configurations, by relatively low core stiffnesses. These capabilities have been exploited to derive a number of results that provide a useful benchmark for future investigations on these structures.

The vibration analysis has been discussed with regard to monolithic configurations, illustrating close agreement between results obtained with the present formulation and those available in the literature.

With regard to buckling analysis, the investigation was confined to sandwich configurations, for which a small number of results is available in the literature. As opposed to straight fiber configurations, the analysis of thick plates should be carefully carried out, as many configurations may suffer from undesired local instabilities. The results clearly illustrate that ED2 theory lead to highly inaccurate predictions in most of the cases. Therefore, a careful selection of the plate theory is recommended. For typical aerospace materials, ED4 theory can be adequate provided the core is moderately stiff. On the other hand, a layerwise theory is necessary when dealing with low density cores, characterized by small transverse shear stiffness.

Future work will be directed towards the introduction of efficient techniques to capture local modes that may characterize the response of sandwich panels.

References

[1] A.W. Leissa and A.F. Martin. Vibration and buckling of rectangular composite plates with variable fiber spacing. *Composite Structures*, 14(4):339–357, 1990.

[2] M.T. DiNardo and P. Lagace. Buckling and postbuckling of laminated composite plates with ply dropoffs. *AIAA Journal*, 27(10):1392–1398, 1989.

[3] M.W. Hyer and R.F. Charette. Use of curvilinear fiber format in composite structure design. In 30^{th} *AIAA Structures, Structural Dynamics, and Materials Conference*, 89-1404-CP, Mobile, AL, 3–5 April 1989.

[4] M.W. Hyer and R.F. Charette. Use of curvilinear fiber format in composite structure design. *AIAA Journal*, 29(6):1011–1015, 1991.

[5] Z. Gürdal and R. Olmedo. Composite laminates with spatially varying fiber orientations: variable stiffness panel concept. In 33^{rd} *AIAA/ASME/ASCE/AHS/ASC Structures, Structural Dynamics and Material Conference*, Dallas, TX, April 13–15 1992.

[6] Z. Gürdal and R. Olmedo. In-plane response of laminates with spatially varying fiber orientations-variable stiffness concept. *AIAA Journal*, 31(4):751–758, 1993.

[7] R. Olmedo and Z. Gürdal. Buckling response of laminates with spatially varying fiber orientations. In 34^{th} *AIAA/ASME/ASCE/AHS/ASC Structures, Structural Dynamics and Material Conference*, La Jolla, CA, April 19–22 1993.

[8] P. Ribeiro, H. Akhavan, A. Teter, and J. Warmiński. A review on the mechanical behaviour of curvilinear fibre composite laminated panels. *Journal of Composite Materials*, 48(22):2761–2777, 2013.

[9] M.M. Abdalla, S. Setoodeh, and Z. Gürdal. Design of variable stiffness composite panels for maximum fundamental frequency using lamination parameters. *Composite Structures*, 81(2):283–291, 2007.

[10] A.W. Blom, S. Setoodeh, J.M. Hol, and Z. Gürdal. Design of variable-stiffness conical shells for maximum fundamental eigenfrequency. *Computers & Structures*, 86(9):870–878, 2008.

[11] S. Honda and Y. Narita. Vibration design of laminated fibrous composite plates with local anisotropy induced by short fibers and curvilinear fibers. *Composite Structures*, 93(2):902–910, 2011.

[12] H. Akhavan and P. Ribeiro. Natural modes of vibration of variable stiffness composite laminates with curvilinear fibers. *Composite Structures*, 93(11):3040–3047, 2011.

[13] F. Tornabene, N. Fantuzzi, M. Bacciocchi, and E. Viola. Higher-order theories for the free vibrations of doubly-curved laminated panels with curvilinear reinforcing fibers by means of a local version of the gdq method. *Composites Part B: Engineering*, 81:196–230, 2015.

[14] B.F. Tatting and Z. Gürdal. Analysis and design of tow-steered variable stiffness composite laminates. In *AHS Meeting*, Williamsburg, VA, 30 October–1 November 2001.

[15] C. Waldhart, Z. Gürdal, and C. Ribbens. Analysis of tow placed, parallel fiber, variable stiffness laminates. In 37^{th} *AIAA Structures, Structural Dynamics, and Materials Conference*, AIAA-96-1569, Salt Lake City, UT, 15–17 April 1996.

[16] S. Setoodeh, M.M. Abdalla, S.T. IJsselmuiden, and Z. Gürdal. Design of variable-stiffness composite panels for maximum buckling load. *Composite Structures*, 87(1):109–117, 2009.

[17] G. Raju, Z. Wu, B.C. Kim, and P.M. Weaver. Prebuckling and buckling analysis of variable angle tow plates with general boundary conditions. *Composite Structures*, 94(9):2961–2970, 2012.

[18] Z. Wu, P.M. Weaver, G. Raju, and B.C. Kim. Buckling analysis and optimisation of variable angle tow composite plates. *Thin-Walled Structures*, 60:163–172, 2012.

[19] Z. Wu, G. Raju, and P.M. Weaver. Postbuckling analysis of variable angle tow composite plates. *International Journal of Solids and Structures*, 50(10):1770–1780, 2013.

[20] C. Bisagni and R. Vescovini. Fast tool for buckling analysis and optimization of stiffened panels. *Journal of Aircraft*, 46(6):2041–2053, 2009.

[21] C. Bisagni and R. Vescovini. Analytical formulation for local buckling and post-buckling analysis of stiffened laminated panels. *Thin-Walled Structures*, 47(3):318–334, 2009.

[22] B.H. Coburn, Z. Wu, and P.M. Weaver. Buckling analysis of stiffened variable angle tow panels. *Composite Structures*, 111:259–270, 2014.

[23] B.H. Coburn and P.M. Weaver. Buckling analysis, design and optimisation of variable stiffness sandwich panels. In *20th International Conference on Composite Materials*, Copenhagen, July 19–24 2015.

[24] J.N. Reddy and N.D. Phan. Stability and vibration of isotropic, orthotropic and laminated plates according to a higher-order shear deformation theory. *Journal of Sound and Vibration*, 98(2):157–170, 1985.

[25] J.N. Reddy. *Mechanics of Laminated Composite Plates and Shells: Theory and Analysis*. CRC Press, Boca Raton, 2004.

[26] A.J.M. Ferreira, C.M.C Roque, A.M.A Neves, R.M.N Jorge, C.M Mota Soares, and J.N. Reddy. Buckling analysis of isotropic and laminated plates by radial basis functions according to a higher-order shear deformation theory. *Thin-Walled Structures*, 49(7):804–811, 2011.

[27] E. Carrera. A class of two-dimensional theories for anisotropic multilayered plates analysis. *Atti Accademia delle Scienze di Torino. Memorie Scienze Fisiche*, 19:1–39, 1995.

[28] E. Carrera. Theories and finite elements for multilayered, anisotropic, composite plates and shells. *Archives of Computational Methods in Engineering*, 9(2):87–140, 2002.

[29] M. D'Ottavio and E. Carrera. Variable-kinematics approach for linearized buckling analysis of laminated plates and shells. *AIAA Journal*, 48(9):1987–1996, 2010.

[30] R. Vescovini and L. Dozio. Exact refined buckling solutions for laminated plates under uniaxial and biaxial loads. *Composite Structures*, 127:356–368, 2015.

[31] A.J.M. Ferreira, C.M.C. Roque, E. Carrera, and M. Cinefra. Analysis of thick isotropic and cross-ply laminated plates by radial basis functions and a unified formulation. *Journal of Sound and Vibration*, 330(4):771–787, 2011.

[32] A.M.A. Neves, A.J.M. Ferreira, E. Carrera, M. Cinefra, R.M.N. Jorge, and C.M.M. Soares. Buckling analysis of sandwich plates with functionally graded skins using a new quasi-3d hyperbolic sine shear deformation theory and collocation with radial basis functions. *ZAMM-Journal of Applied Mathematics and Mechanics/Zeitschrift für Angewandte Mathematik und Mechanik*, 92(9):749–766, 2012.

[33] A.M.A. Neves, A.J.M. Ferreira, E. Carrera, M. Cinefra, C.M.C. Roque, R.M.N. Jorge, and C.M.M. Soares. Static, free vibration and buckling analysis of isotropic and sandwich functionally graded plates using a quasi-3d higher-order shear deformation theory and a meshless technique. *Composites Part B: Engineering*, 44(1):1657–674, 2013.

[34] A.J.M. Ferreira. A formulation of the multiquadric radial basis function method for the analysis of laminated composite plates. *Composite Structures*, 59(3):385–392, 2003.

[35] A. Pagani, E. Carrera, and A.J.M. Ferreira. Higher-order theories and radial basis functions applied to free vibration analysis of thin-walled beams. *Mechanics of Advanced Materials and Structures*, 2014.

[36] F.A. Fazzolari and E. Carrera. Advanced variable kinematics ritz and galerkin formulations for accurate buckling and vibration analysis of anisotropic laminated composite plates. *Composite Structures*, 94(1):50–67, 2011.

[37] F.A. Fazzolari and E. Carrera. Thermo-mechanical buckling analysis of anisotropic multilayered composite and sandwich plates by using refined variable-kinematics theories. *Journal of Thermal Stresses*, 36(4):321–350, 2013.

[38] L. Dozio and R. Vescovini. Refined buckling analysis of composite plates under various boundary conditions. In *18th International Conference on Composite Structures (ICCS18)*, Lisbon, June 15–18 2015.

[39] E. Carrera, F.A. Fazzolari, and L. Demasi. Vibration analysis of anisotropic simply supported plates by using variable kinematic and rayleigh-ritz method. *Journal of Vibration and Acoustics*, 133(6):061017–1–061017–16, 2011.

[40] L. Dozio and E. Carrera. Ritz analysis of vibrating rectangular and skew multilayered plates based on advanced variable-kinematic models. *Composite Structures*, 94(6):2118–2128, 2012.

[41] R.M.J. Groh, P.M. Weaver, S. White, G. Raju, and Z. Wu. A 2D equivalent single-layer formulation for the effect of transverse shear on laminated plates with curvilinear fibres. *Composite Structures*, 100:464–478, 2013.

[42] L. Dozio. Exact vibration solutions for cross-ply laminated plates with two opposite edges simply supported using refined theories of variable order. *Journal of Sound and Vibration*, 333(8):2347–2359, 2014.

[43] A. Alhajahmad, M.M. Abdalla, and Z. Gürdal. Design tailoring for pressure pillowing using tow-placed steered fibers. *Journal of Aircraft*, 45(2):630–640, 2008.

[44] S. Nagendra, S. Kodiyalam, J.E. Davis, and V.N. Parthasarathy. Optimization of tow fiber paths for composite design. In 36^{th} *AIAA Structures, Structural Dynamics, and Materials Conference*, New Orleans, LA, April 10–12 1995.

[45] Z. Gürdal, B.F. Tatting, and C.K. Wu. Variable stiffness composite panels: effects of stiffness variation on the in-plane and buckling response. *Composites Part A: Applied Science and Manufacturing*, 39(5):911–922, 2008.

[46] R. Vescovini and C. Bisagni. Single-mode solution for post-buckling analysis of composite panels with elastic restraints loaded in compression. *Composites Part B: Engineering*, 43(3):1258–1274, 2012.

[47] R. Vescovini and C. Bisagni. Two-step procedure for fast post-buckling analysis of composite stiffened panels. *Computers & Structures*, 128:38–47, 2013.

[48] Hexcel website. `http://www.hexcel.com`.

[49] W.S. Burton and A.K. Noor. Assessment of continuum models for sandwich panel honeycomb cores. *Computer Methods in Applied Mechanics and Engineering*, 145(3):341–360, 1997.

[50] C. Bisagni, R. Vescovini, and C.G. Dávila. Single-stringer compression specimen for the assessment of damage tolerance of postbuckled structures. *Journal of Aircraft*, 48(2):495–502, 2011.

Table 1: Material properties.

	E_{11} (MPa)	$E_{22} = E_{33}$ (MPa)	G_{12} (MPa)	$G_{13} = G_{23}$ (MPa)	$\nu_{12} = \nu_{13} = \nu_{23}$	ρ (kg/m^3)
Material 1 [12]	173000	7200	3760	3760	0.29	1540
Material 2 [50]	150000	9080	5290	5290	0.32	1500

Table 2: Aluminum honey-comb properties.

	E_{11} (MPa)	E_{22} (MPa)	E_{33} (MPa)	G_{12} (MPa)	G_{13} (MPa)	G_{23} (MPa)	ν_{12}	ν_{23}	ν_{13}	ρ (kg/m^3)
Core H	12	12	4608	7	1108	664	0.99	7.74E-4	7.76E-4	192
Core L	0.44	0.44	1536	0.27	369	222	0.99	8.64E-5	8.64E-5	72

Table 3: Preliminary convergence study. Nondimensional frequencies $\overline{\omega} = \omega \frac{a^2}{h}\sqrt{\frac{\rho}{E_2}}$ for SSSS square panel of Material 1, b/h=50 and ED4 theory.

		Mode 1	Mode 2	Mode 3	Mode 4
Lay-up	P				
$[0\ 90]_s$	4	14.9132	32.5111	64.6213	72.1250
	6	14.9092 (0.03%)	27.4667 (18.37%)	52.2277 (23.73%)	53.8552 (33.92%)
	8	14.9092 (0.00%)	27.3893 (0.28%)	52.0283 (0.38%)	53.0845 (1.45%)
	10	14.9092 (0.00%)	27.3889 (0.00%)	52.0275 (0.00%)	53.0734 (0.02%)
	12	14.9092 (0.00%)	27.3889 (0.00%)	52.0275 (0.00%)	53.0733 (0.00%)
	14	14.9092 (0.00%)	27.3889 (0.00%)	52.0275 (0.00%)	53.0733 (0.00%)
$[\pm<0\|90>_x]_s$	4	15.0289	31.8338	39.3170	61.3495
	6	14.9388 (0.60%)	29.8993 (6.47%)	35.3807 (11.13%)	51.1092 (20.04%)
	8	14.7653 (1.18%)	29.1777 (2.47%)	34.5653 (2.36%)	49.5730 (3.10%)
	10	14.7223 (0.29%)	28.9304 (0.85%)	34.4787 (0.25%)	49.4232 (0.30%)
	12	14.7093 (0.09%)	28.8895 (0.14%)	34.4741 (0.01%)	49.2867 (0.28%)
	14	14.7030 (0.04%)	28.8471 (0.15%)	34.4683 (0.02%)	49.1892 (0.20%)

Table 4: Nondimensional frequencies $\overline{\omega} = \omega \frac{a^2}{h}\sqrt{\frac{\rho}{E_2}}$ for SSSS square panel of Material 1 and lay-up [<0|45>$_x$,<-45|-60>$_x$,<0|45>$_x$].

Method	Mode			
	1	2	3	4
			b/h=100	
p-version Ref. [12]	16.5794	27.2818	44.4149	49.7264
LGDQ Ref. [13]	16.5198	27.2333	44.4729	49.7333
ED2	16.5234 (-0.34%)	27.2558 (-0.10%)	44.4554 (0.09%)	49.6648 (-0.12%)
ED3	16.5140 (-0.39%)	27.2369 (-0.16%)	44.4185 (0.01%)	49.6057 (-0.24%)
ED4	16.5140 (-0.39%)	27.2368 (-0.16%)	44.4183 (0.01%)	49.6056 (-0.24%)
LD1	16.5326 (-0.28%)	27.2924 (0.04%)	44.5381 (0.28%)	49.6693 (-0.11%)
LD2	16.5097 (-0.42%)	27.2268 (-0.20%)	44.4032 (-0.03%)	49.6009 (-0.25%)
LD3	16.5073 (-0.43%)	27.2212 (-0.22%)	44.3940 (-0.05%)	49.5976 (-0.26%)
			b/h=10	
p-version Ref. [12]	13.5724	21.6825	32.3781	33.8731
LGDQ Ref. [13]	13.1984	21.3644	32.2639	33.9147
ED2	13.8819 (2.28%)	22.3681 (3.16%)	33.7378 (4.20%)	35.2302 (4.01%)
ED3	13.5109 (-0.45%)	21.6430 (-0.18%)	32.3415 (-0.11%)	33.8929 (0.06%)
ED4	13.5092 (-0.47%)	21.6388 (-0.20%)	32.3346 (-0.13%)	33.8820 (0.03%)
LD1	13.6429 (0.52%)	21.7867 (0.48%)	33.0235 (1.99%)	34.0464 (0.51%)
LD2	13.4563 (-0.86%)	21.5043 (-0.82%)	32.2795 (-0.30%)	33.6341 (-0.71%)
LD3	13.4248 (-1.09%)	21.4215 (-1.20%)	32.2222 (-0.48%)	33.4725 (-1.18%)

Table 5: Nondimensional frequencies $\overline{\omega} = \omega \frac{a^2}{h}\sqrt{\frac{\rho}{E_2}}$ for CCCC square panel of Material 1 and lay-up [<0|45>$_x$,<-45|-60>$_x$,<0|45>$_x$].

Method	Mode			
	1	2	3	4
			b/h=100	
p-version Ref. [12]	26.7961	37.9943	56.6905	69.0836
LGDQ Ref. [13]	26.8169	38.0153	56.7368	69.1492
ED2	26.8551 (0.22%)	38.0957 (0.27%)	56.8668 (0.31%)	69.2721 (0.27%)
ED3	26.8207 (0.09%)	38.0476 (0.14%)	56.7876 (0.17%)	69.0869 (0.00%)
ED4	26.8206 (0.09%)	38.0475 (0.14%)	56.7874 (0.17%)	69.0868 (0.00%)
LD1	26.8660 (0.26%)	38.1408 (0.39%)	56.9571 (0.47%)	69.2377 (0.22%)
LD2	26.8195 (0.09%)	38.0431 (0.13%)	56.7760 (0.15%)	69.0844 (0.00%)
LD3	26.8185 (0.08%)	38.0397 (0.12%)	56.7675 (0.14%)	69.0809 (0.00%)
			b/h=10	
p-version Ref. [12]	17.8361	26.4167	35.8115	38.8788
LGDQ Ref. [13]	17.7153	26.2884	35.2717	38.6484
ED2	18.3970 (3.14%)	27.3532 (3.55%)	36.9474 (3.17%)	40.5168 (4.21%)
ED3	17.7105 (-0.70%)	26.3003 (-0.44%)	35.2853 (-1.47%)	38.6864 (-0.49%)
ED4	17.7060 (-0.73%)	26.2896 (-0.48%)	35.2693 (-1.51%)	38.6631 (-0.55%)
LD1	18.0218 (1.04%)	26.5922 (0.66%)	36.0833 (0.76%)	38.9697 (0.23%)
LD2	17.6720 (-0.92%)	26.1759 (-0.91%)	35.2267 (-1.63%)	38.4079 (-1.21%)
LD3	17.6327 (-1.14%)	26.0790 (-1.28%)	35.1348 (-1.89%)	38.2083 (-1.72%)

Table 6: Nondimensional frequencies $\overline{\omega} = \omega \frac{a^2}{h}\sqrt{\frac{\rho^{\text{face}}}{E_2}}$ for CFFF sandwich panel with face-sheet of Material 1 and lay-up [<0|45>$_x$,<-45|-60>$_x$,<0|45>$_x$], and Core L with h_{f}/h=0.10.

a/b	Theory	Mode				Mode				Mode			
		1	2	3	4	1	2	3	4	1	2	3	4
		b/h=100				b/h=50				b/h=10			
1	ED2	4.1429	9.7631	24.2744	32.5761	4.1002	9.5788	23.7127	31.8724	3.6821	7.9407	11.9758	18.1479
	ED4	4.1142	9.6468	23.9209	32.1586	4.0417	9.3462	22.9283	30.6815	3.3610	6.8627	11.9512	14.9936
	LD1	4.1081	9.6257	23.8531	32.0692	4.0301	9.3048	22.7834	30.4486	3.3105	6.7041	11.9451	14.5445
	LD2	4.1081	9.6257	23.8528	32.0689	4.0300	9.3047	22.7828	30.4476	3.3093	6.7013	11.9423	14.5318
	Abaqus	4.0924	9.6315	23.9126	32.0361	4.0120	9.3128	22.8421	30.4028	3.3477	6.9041	11.5623	15.0779
2	ED2	3.8657	16.3793	30.0566	53.6760	3.8265	16.1481	29.8060	52.9823	3.5643	14.1935	15.4039	26.0942
	ED4	3.8409	16.2393	29.9095	53.2596	3.7824	15.8836	29.4262	52.0042	3.3970	12.8589	15.3777	23.0854
	LD1	3.8359	16.2143	29.8781	53.1747	3.7742	15.8373	29.3491	51.8139	3.3704	12.6473	15.3699	22.6068
	LD2	3.8359	16.2141	29.8780	53.1743	3.7741	15.8371	29.3488	51.8131	3.3699	12.6455	15.3671	22.5996
	Abaqus	3.8250	16.2171	29.8703	53.3410	3.7612	15.8460	29.3271	51.9736	3.3728	12.9171	14.8626	23.1550
3	ED2	3.6465	22.3713	30.5915	62.8547	3.6067	22.1080	30.3972	62.2630	3.3612	16.2699	19.9127	27.9935
	ED4	3.6229	22.2130	30.4748	62.5038	3.5645	21.8159	30.1325	61.5151	3.2297	16.2496	18.3947	25.9012
	LD1	3.6179	22.1846	30.4496	62.4346	3.5566	21.7648	30.0790	61.3738	3.2101	16.2427	18.1480	25.5419
	LD2	3.6178	22.1845	30.4494	62.4343	3.5566	21.7646	30.0788	61.3730	3.2096	16.2391	18.1462	25.5377
	Abaqus	3.6000	22.1270	30.5229	62.5005	3.5373	21.7200	30.1303	61.4477	3.1980	15.6472	18.4272	25.9416

Table 7: Convergence study. Nondimensional buckling force per unit length $\overline{N}_x = \dfrac{N_{x,\text{avg}}a^2}{E_1 h^3}$ for Case B, SSSS square panel of Material 2, b/h=50 and ED4 theory.

	$[0\ 90]_\text{s}$	$[\pm<90\|0>_y]_\text{s}$
P		
4	1.0163	2.2447
6	1.0158 (0.05%)	2.2252 (0.88%)
8	1.0158 (0.00%)	2.1230 (4.81%)
10	1.0158 (0.00%)	2.0980 (1.19%)
12	1.0158 (0.00%)	2.0925 (0.26%)
14	1.0158 (0.00%)	2.0898 (0.13%)

Table 8: Nondimensional buckling force $\overline{N}_x = \dfrac{N_{x,\text{avg}}a^2}{E_1h^3}$ for Case B square sandwich panels with face-sheet of Material 2 and lay-up $[<45|30>_y]_2$ and Core L.

b/h	Theory	Boundary conditions				Boundary conditions			
		SSSS	CSCS	CSCF	CCCC	SSSS	CSCS	CSCF	CCCC
		h_f/h=0.05				h_f/h=0.10			
100	ED2	0.5546	0.8599	0.4186	1.1049	0.9941	1.5401	0.7498	1.9768
	ED4	0.5491	0.8457	0.4104	1.0789	0.9798	1.4971	0.7241	1.8978
	LD1	0.5474	0.8416	0.4084	1.0720	0.9754	1.4857	0.7186	1.8771
	LD2	0.5474	0.8416	0.4084	1.0720	0.9754	1.4857	0.7186	1.8771
	Abaqus	0.5473	0.8427	0.4087	1.0711	0.9753	1.4873	0.7191	1.8743
50	ED2	0.5467	0.8332	0.4010	1.0583	0.9788	1.4880	0.7159	1.8870
	ED4	0.5319	0.7923	0.3820	0.9858	0.9301	1.3502	0.6516	1.6519
	LD1	0.5281	0.7827	0.3778	0.9699	0.9174	1.3192	0.6388	1.6006
	LD2	0.5281	0.7827	0.3778	0.9698	0.9173	1.3191	0.6388	1.6004
	Abaqus	0.5288	0.7859	0.3793	0.9708	0.9189	1.3233	0.6407	1.5978
25	ED2	0.5176	0.7438	0.3557	0.9142	0.9227	1.3155	0.6288	1.6121
	ED4	0.4729	0.6388	0.3124	0.7458	0.7739	0.9810	0.4881	1.1043
	LD1	0.4633	0.6181	0.3038	0.7157	0.7422	0.9230	0.4650	1.0237
	LD2	0.4633	0.6179	0.3037	0.7152	0.7418	0.9225	0.4648	1.0227
	Abaqus	0.4661	0.6245	0.3073	0.7186	0.7465	0.9271	0.4683	1.0176

Table 9: Nondimensional buckling force $\overline{N}_x = \dfrac{N_{x,\text{avg}}a^2}{E_1 h^3}$ for Case B square sandwich panels with face-sheet of Material 2, b/h=50 and h_f/h=0.10.

Face-sheet	Theory	Boundary conditions				Boundary conditions			
		SSSS	CSCS	CSCF	CCCC	SSSS	CSCS	CSCF	CCCC
		Core H				Core L			
$[\pm 45]_2$	ED2	0.8521	1.1759	0.5689	1.6100	0.8402	1.1510	0.5564	1.5653
	ED4	0.8384	1.1439	0.5557	1.5367	0.7946	1.0436	0.5154	1.3345
	LD1	0.8354	1.1374	0.5532	1.5228	0.7827	1.0189	0.5068	1.2855
	LD2	0.8351	1.1370	0.5530	1.5222	0.7827	1.0189	0.5068	1.2854
	Abaqus	0.8370	1.1419	0.5550	1.5270	0.7847	1.0229	0.5084	1.2852
$[\pm<45\|30>_y]_2$	ED2	0.9946	1.5228	0.7310	1.9428	0.9788	1.4880	0.7159	1.8870
	ED4	0.9797	1.4829	0.7123	1.8697	0.9301	1.3502	0.6516	1.6519
	LD1	0.9764	1.4748	0.7086	1.8556	0.9174	1.3192	0.6388	1.6006
	LD2	0.9760	1.4743	0.7085	1.8549	0.9173	1.3191	0.6388	1.6004
	Abaqus	0.9775	1.4799	0.7110	1.8574	0.9189	1.3233	0.6407	1.5978
$[\pm<75\|15>_y]_2$	ED2	1.3649	1.7539	0.5919	2.5079	1.3794	1.7584	0.5734	2.5198
	ED4	1.3424	1.7078	0.5752	2.3981	1.3093	1.6000	0.5119	2.1534
	LD1	1.3375	1.6983	0.5719	2.3775	1.2904	1.5625	0.4998	2.0714
	LD2	1.3367	1.6974	0.5718	2.3761	1.2903	1.5624	0.4998	2.0711
	Abaqus	1.3445	1.7118	0.5752	2.3863	1.2978	1.5733	0.5026	2.0669

Table 10: Nondimensional buckling force $\overline{N}_x = \dfrac{N_x a^2}{E_1 h^3}$ for Case A square sandwich panels with face-sheet of Material 2, b/h=50 and h_{f}/h=0.10.

Face-sheet	Theory	Boundary conditions				Boundary conditions			
		SSSS	CSCS	CSCF	CCCC	SSSS	CSCS	CSCF	CCCC
		Core H				Core L			
$[\pm 45]_2$	ED2	0.8521	1.1759	0.5689	1.6100	0.8402	1.1510	0.5564	1.5653
	ED4	0.8384	1.1439	0.5557	1.5367	0.7946	1.0436	0.5154	1.3345
	LD1	0.8354	1.1374	0.5532	1.5228	0.7827	1.0189	0.5068	1.2855
	LD2	0.8351	1.1370	0.5530	1.5222	0.7827	1.0189	0.5068	1.2854
	Abaqus	0.8370	1.1419	0.5550	1.5270	0.7847	1.0229	0.5084	1.2852
$[\pm<0\|30>_x]_2$	ED2	0.7024	1.5558	1.3269	1.6976	0.6879	1.5111	1.2953	1.6426
	ED4	0.6928	1.5121	1.2910	1.6478	0.6566	1.3458	1.1556	1.4618
	LD1	0.6907	1.5033	1.2839	1.6379	0.6490	1.3122	1.1276	1.4246
	LD2	0.6904	1.5029	1.2837	1.6373	0.6489	1.3122	1.1276	1.4245
	Abaqus	0.6919	1.5098	1.2884	1.6434	0.6505	1.3168	1.1306	1.4279
$[\pm<0\|60>_x]_2$	ED2	0.9030	1.3387	0.8347	1.5973	0.8741	1.2805	0.8115	1.5162
	ED4	0.8887	1.3038	0.8165	1.5480	0.8270	1.1673	0.7502	1.3648
	LD1	0.8856	1.2969	0.8129	1.5385	0.8153	1.1432	0.7374	1.3325
	LD2	0.8852	1.2964	0.8126	1.5377	0.8152	1.1431	0.7373	1.3324
	Abaqus	0.8876	1.3032	0.8159	1.5421	0.8176	1.1485	0.7400	1.3337

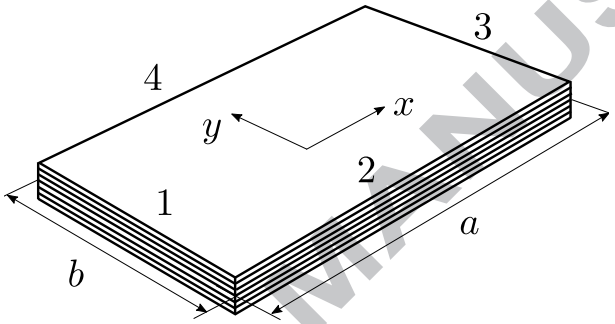

Figure 1: Multilayered plate dimensions and reference system.

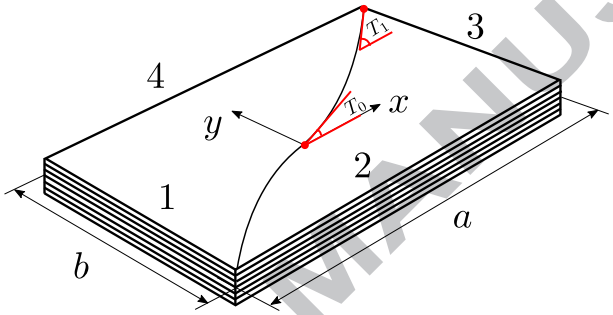

Figure 2: Fiber passing through the origin and linearly varying orientation along x.

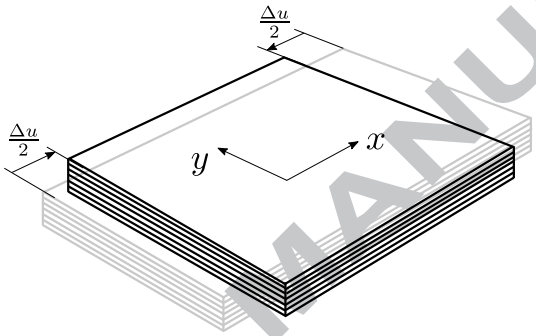

Figure 3: Undeformed (gray) and deformed (black) configurations in the pre-buckling state.

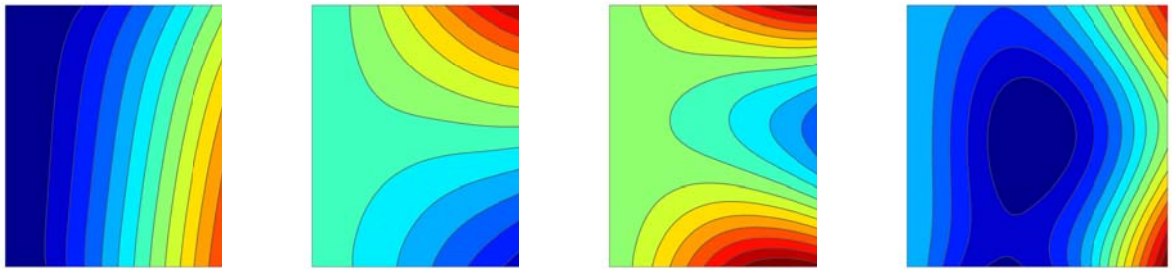

(a) Mode 1 (b) Mode 2 (c) Mode 3 (d) Mode 4

Figure 4: First four vibration modes of CFFF sandwich panels with b/h=100 and a/b=1. Contour of the out of plane displacement.

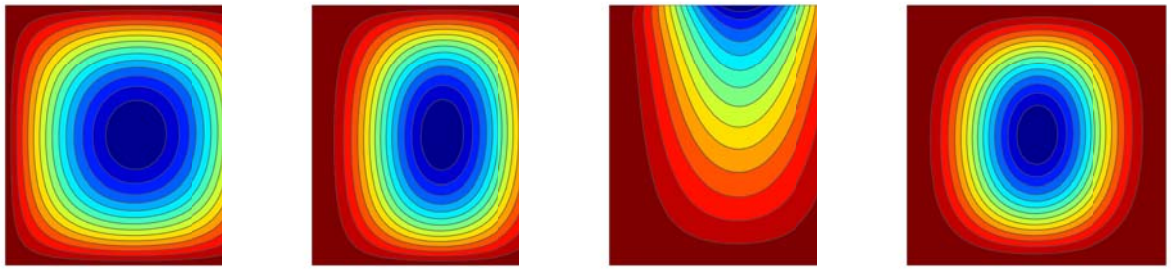

(a) SSSS (b) CSCS (c) CSCF (d) CCCC

Figure 5: Buckling modes of square sandwich panels with face-sheet $\pm[<45|30>]_s$ for different boundary conditions. Contour of the out of plane displacement.

6 APPENDIX

Define the terms:

$$X^{ef}_{\alpha m\beta\overline{m}} = \frac{\mathrm{d}^e}{\mathrm{d}\xi^e}\left[\Phi_{\alpha\tau m}\right]\frac{\mathrm{d}^f}{\mathrm{d}\xi^f}\left[\Phi_{\beta\overline{s}\overline{m}}\right] \quad m,\overline{m} = 1,2,\ldots,P \tag{44}$$

$$Y^{ef}_{\alpha m\beta\overline{m}} = \frac{\mathrm{d}^e}{\mathrm{d}\eta^e}\left[\Psi_{\alpha\tau m}\right]\frac{\mathrm{d}^f}{\mathrm{d}\eta^f}\left[\Psi_{\beta\overline{s}\overline{m}}\right] \quad n,\overline{n} = 1,2,\ldots,P \tag{45}$$

Stiffness matrix nucleus

$$K^k_{\tau sij}(1,1) = \int_S \Big[E^k_{\tau s}\frac{b}{a}\tilde{C}^k_{11}X^{11}_{umu\overline{m}}Y^{00}_{unu\overline{n}} + E^k_{\tau s}\tilde{C}^k_{16}\left(X^{10}_{umu\overline{m}}Y^{01}_{unu\overline{n}} + X^{01}_{umu\overline{m}}Y^{10}_{unu\overline{n}}\right) + E^k_{\tau s}\frac{a}{b}\tilde{C}^k_{66}X^{00}_{umu\overline{m}}Y^{11}_{unu\overline{n}} + E^k_{\tau_z s_z}\frac{ab}{4}\tilde{C}^k_{55}X^{00}_{umu\overline{m}}Y^{00}_{unu\overline{n}}\Big]\,\mathrm{d}S$$

$$K^k_{\tau sij}(1,2) = \int_S \Big[E^k_{\tau s}\frac{b}{a}\tilde{C}^k_{16}X^{11}_{umv\overline{m}}Y^{00}_{unv\overline{n}} + E^k_{\tau s}(\tilde{C}^k_{12}X^{10}_{umv\overline{m}}Y^{01}_{unv\overline{n}} + \tilde{C}^k_{66}X^{01}_{umv\overline{m}}Y^{10}_{unv\overline{n}}) + E^k_{\tau s}\frac{a}{b}\tilde{C}^k_{26}X^{00}_{umv\overline{m}}Y^{11}_{unv\overline{n}} + E^k_{\tau_z s_z}\frac{ab}{4}\tilde{C}^k_{45}X^{00}_{umv\overline{m}}Y^{00}_{unv\overline{n}}\Big]\,\mathrm{d}S$$

$$K^k_{\tau sij}(1,3) = \int_S \Big[E^k_{\tau s_z}\frac{b}{2}\tilde{C}^k_{13}X^{10}_{umw\overline{m}}Y^{00}_{unw\overline{n}} + E^k_{\tau_z s}\frac{b}{2}\tilde{C}^k_{55}X^{01}_{umw\overline{m}}Y^{00}_{unw\overline{n}} + E^k_{\tau s_z}\frac{a}{2}\tilde{C}^k_{36}X^{00}_{umw\overline{m}}Y^{10}_{unw\overline{n}} + E^k_{\tau_z s}\frac{a}{2}\tilde{C}^k_{45}X^{00}_{umw\overline{m}}Y^{01}_{unw\overline{n}}\Big]\,\mathrm{d}S$$

$$K^k_{\tau sij}(2,1) = \int_S \Big[E^k_{\tau s}\frac{b}{a}\tilde{C}^k_{16}X^{11}_{vmu\overline{m}}Y^{00}_{vnu\overline{n}} + E^k_{\tau s}(\tilde{C}^k_{12}X^{01}_{vmu\overline{m}}Y^{10}_{vnu\overline{n}} + \tilde{C}^k_{66}X^{10}_{vmu\overline{m}}Y^{01}_{vnu\overline{n}}) + E^k_{\tau s}\frac{a}{b}\tilde{C}^k_{26}X^{00}_{vmu\overline{m}}Y^{11}_{vnu\overline{n}} + E^k_{\tau_z s_z}\frac{ab}{4}\tilde{C}^k_{45}X^{00}_{vmu\overline{m}}Y^{00}_{vnu\overline{n}}\Big]\,\mathrm{d}S$$

$$K^k_{\tau sij}(2,2) = \int_S \Big[E^k_{\tau s}\frac{b}{a}\tilde{C}^k_{66}X^{11}_{vmv\overline{m}}Y^{00}_{vnv\overline{n}} + E^k_{\tau s}(\tilde{C}^k_{26}X^{10}_{vmv\overline{m}}Y^{01}_{vnv\overline{n}} + \tilde{C}^k_{26}X^{01}_{vmv\overline{m}}Y^{10}_{vnv\overline{n}}) + E^k_{\tau s}\frac{a}{b}\tilde{C}^k_{22}X^{00}_{vmv\overline{m}}Y^{11}_{vnv\overline{n}} + E^k_{\tau_z s_z}\frac{ab}{4}\tilde{C}^k_{44}X^{00}_{vmv\overline{m}}Y^{00}_{vnv\overline{n}}\Big]\,\mathrm{d}S$$

$$K^k_{\tau sij}(2,3) = \int_S \Big[E^k_{\tau s_z}\frac{b}{2}\tilde{C}^k_{36}X^{10}_{vmw\overline{m}}Y^{00}_{vnw\overline{n}} + E^k_{\tau_z s}\frac{b}{2}\tilde{C}^k_{45}X^{01}_{vmw\overline{m}}Y^{00}_{vnw\overline{n}} + E^k_{\tau s_z}\frac{a}{2}\tilde{C}^k_{23}X^{00}_{vmw\overline{m}}Y^{10}_{vnw\overline{n}} + E^k_{\tau_z s}\frac{a}{2}\tilde{C}^k_{44}X^{00}_{vmw\overline{m}}Y^{01}_{vnw\overline{n}}\Big]\,\mathrm{d}S$$

$$K^k_{\tau sij}(3,1) = \int_S \Big[E^k_{\tau s_z}\frac{b}{2}\tilde{C}^k_{55}X^{10}_{wmu\overline{m}}Y^{00}_{wnu\overline{n}} + E^k_{\tau_z s}\frac{b}{2}\tilde{C}^k_{13}X^{01}_{wmu\overline{m}}Y^{00}_{wnu\overline{n}} + E^k_{\tau s_z}\frac{a}{2}\tilde{C}^k_{45}X^{00}_{wmu\overline{m}}Y^{10}_{wnu\overline{n}} + E^k_{\tau_z s}\frac{a}{2}\tilde{C}^k_{36}X^{00}_{wmu\overline{m}}Y^{01}_{wnu\overline{n}}\Big]\,\mathrm{d}S$$

$$K^k_{\tau sij}(3,2) = \int_S \Big[E^k_{\tau s_z}\frac{b}{2}\tilde{C}^k_{45}X^{10}_{wmv\overline{m}}Y^{00}_{wnv\overline{n}} + E^k_{\tau_z s}\frac{b}{2}\tilde{C}^k_{36}X^{01}_{wmv\overline{m}}Y^{00}_{wnv\overline{n}} + E^k_{\tau s_z}\frac{a}{2}\tilde{C}^k_{44}X^{00}_{wmv\overline{m}}Y^{10}_{wnv\overline{n}} + E^k_{\tau_z s}\frac{a}{2}\tilde{C}^k_{23}X^{00}_{wmv\overline{m}}Y^{01}_{wnv\overline{n}}\Big]\,\mathrm{d}S$$

$$K^k_{\tau sij}(3,3) = \int_S \Big[E^k_{\tau s}\frac{b}{a}\tilde{C}^k_{55}X^{11}_{wmw\overline{m}}Y^{00}_{wnw\overline{n}} + E^k_{\tau s}(\tilde{C}^k_{45}X^{10}_{wmw\overline{m}}Y^{01}_{wnw\overline{n}} + \tilde{C}^k_{45}X^{01}_{wmw\overline{m}}Y^{10}_{wnw\overline{n}}) + E^k_{\tau s}\frac{a}{b}\tilde{C}^k_{44}X^{00}_{wmw\overline{m}}Y^{11}_{wnw\overline{n}} + E^k_{\tau_z s_z}\frac{ab}{4}\tilde{C}^k_{33}X^{00}_{wmw\overline{m}}Y^{00}_{wnw\overline{n}}\Big]\,\mathrm{d}S$$

Mass matrix nucleus

$$M^k_{\tau sij}(1,1) = E^k_{\tau s}\rho\frac{ab}{4}\int_S X^{00}_{mu\overline{m}u}Y^{00}_{unu\overline{n}}\,\mathrm{d}S$$

$$M^k_{\tau sij}(2,2) = E^k_{\tau s}\rho\frac{ab}{4}\int_S X^{00}_{mv\overline{m}v}Y^{00}_{vnv\overline{n}}\,\mathrm{d}S$$

$$M^k_{\tau sij}(3,3) = E^k_{\tau s}\rho\frac{ab}{4}\int_S X^{00}_{mw\overline{m}w}Y^{00}_{wnw\overline{n}}\,\mathrm{d}S$$

Geometric matrix nucleus

$$G^k_{\tau sij}(1,1) = E^k_{\tau s}\int_S\left[\varphi\frac{a}{b}\sigma^k_{0yy}X^{00}_{umu\overline{m}}Y^{11}_{unu\overline{n}} + \varphi(\sigma^k_{0xy}X^{10}_{umu\overline{m}}Y^{01}_{unu\overline{n}} + \sigma^k_{0xy}X^{01}_{umu\overline{m}}Y^{10}_{unu\overline{n}}) + \frac{b}{a}\varphi\sigma^k_{0xx}X^{11}_{umu\overline{m}}Y^{00}_{unu\overline{n}}\right]\mathrm{d}S$$

$$G^k_{\tau sij}(2,2) = E^k_{\tau s}\int_S\left[\varphi\frac{a}{b}\sigma^k_{0yy}X^{00}_{vmv\overline{m}}Y^{11}_{vnv\overline{n}} + \varphi(\sigma^k_{0xy}X^{10}_{vmv\overline{m}}Y^{01}_{vnv\overline{n}} + \sigma^k_{0xy}X^{01}_{vmv\overline{m}}Y^{10}_{vnv\overline{n}}) + \frac{b}{a}\varphi\sigma^k_{0xx}X^{11}_{vmv\overline{m}}Y^{00}_{vnv\overline{n}}\right]\mathrm{d}S$$

$$G^k_{\tau sij}(3,3) = E^k_{\tau s}\int_S\left[\frac{a}{b}\sigma^k_{0yy}X^{00}_{wmw\overline{m}}Y^{11}_{wnw\overline{n}} + (\sigma^k_{0xy}X^{10}_{wmw\overline{m}}Y^{01}_{wnw\overline{n}} + \sigma^k_{0xy}X^{01}_{wmw\overline{m}}Y^{10}_{wnw\overline{n}}) + \frac{b}{a}\sigma^k_{0xx}X^{11}_{wmw\overline{m}}Y^{00}_{wnw\overline{n}}\right]\mathrm{d}S$$